Strain rate sensitivity of a $Cu_{60}Zr_{40}$ metallic and nanoglass

A. Sharma[a], S.S. Hirmukhe[b], Sree Harsha Nandam[c,d], Horst Hahn[d,e,f], I. Singh[b], R. Lakshmi Narayan[g], K. Eswar Prasad[a,*]

[a] Department of Metallurgy Engineering and Materials Science, Indian Institute of Technology Indore, Indore 453552, India
[b] Department of Mechanical Engineering, Indian Institute of Technology Indore, Indore 453552, India
[c] Department of Metallurgical Engineering, Indian Institute of Technology (BHU), Varanasi 221005, India
[d] Institute of Nanotechnology, Karlsruhe Institute of Technology, Hermann-von-Helmholtz-Platz 1, 76344 Eggenstein-Leopoldshafen, Germany
[e] Herbert Gleiter Institute of Nanoscience, Nanjing University of Science and Technology, Nanjing, China
[f] KIT-TUD Joint Research Laboratory Nanomaterials, Institute of Materials Science, Technische Universität Darmstadt (TUD), Otto-Berndt-Str. 3, D-64206 Darmstadt, Germany
[g] Department of Materials Science and Engineering, Indian Institute of Technology Delhi, Hauz Khas, New Delhi 110016, India

ARTICLE INFO

Keywords:
Nanoglass
Metallic glass
Strain rate sensitivity
Nanoindentation
Hardness
Plastic flow
Shear bands

ABSTRACT

The strain rate sensitivity, *m*, of a binary Cu_{60} Zr_{40} nanoglass (NG) and metallic glass (MG) are investigated using nanoindentation. Indentations were performed at different loading rates in the range of 0.26–8 mN/s, which gives equivalent indentation strain rates over three decades. The load vs. displacement curves of MG exhibited noticeable displacement bursts at low loading rates, which gradually decreased with increasing loading rate suggesting a transition from more to less severe heterogeneous plastic flow. While in the case of NG, no noticeable displacement bursts are present at any of the loading rates suggesting a near homogeneous plastic flow. In both NG and MG, the hardness decreases with increasing loading rate, resulting in negative strain rate sensitivity, *m*. The *m* for NG is higher than the MG, indicating a more homogeneous flow underneath the indentation. Interface indentation experiments and subsequent analysis of the deformation zone showed a larger number of fine secondary shear bands (SSBs) in NG as compared to the primary shear bands (PSBs), while the plastic flow in MG is accommodated mostly by the PSBs. The findings of the current study will help improve the understanding of the plastic deformation behavior of NGs and provide insights for designing the novel microstructural architecture of amorphous alloys with improved ductility.

1. Introduction

Amorphous alloys, such as metallic glasses (MGs) and bulk metallics glasses (BMGs), exhibit an interesting combination of mechanical properties such as high yield strengths (~ 1 GPa) and large yield strains. However, these advantages are overshadowed by their poor room temperature ductility due to the plastic flow localization into thin shear bands, thereby leading to catastrophic failure [1–3]. When deformed at elevated temperatures (near the glass transition temperature, Tg), the same glasses exhibit extensive plastic flow, which is attributed to the strain partitioning into multiple fine shear bands [4]. To date, different methods have been proposed to improve the room temperature ductility of MGs, of which the notable ones include the fabrication of (*i*) bulk metallic glass matrix composites (BMGMCs) [5] and (*ii*) Nanoglasses (NGs) [6,7]. BMGMCs comprise crystalline phases embedded in an amorphous matrix which appears to resist the unhindered propagation of shear bands in the matrix regions, thereby avoiding catastrophic failure and thus increasing the ductility. However, due to the presence of crystalline phases, the key attributes of a fully amorphous structure cannot be completely exploited. Recently, it was shown that BMGs could also be fabricated using the selective laser melting (SLM) process, which offers distinct shear band characteristics compared to the conventional BMGs but exhibits lower strength and ductility due to the presence of large porosity [8].

Unlike BMGMCs, the newly developed NGs contain a fully amorphous structure with glassy grains (GGs) separated by glassy interfaces (GIs). Similar to the MGs, the fundamental units of plastic deformation in NGs are the shear transformation zones (STZs) which are a cluster of atoms that undergo cumulative shearing under the influence of external load and nucleate in the regions of high free volume [9–11]. In NGs, both the GIs and GGs are the sources of free volume, and hence the probability of finding STZs is much higher

* Corresponding author.
E-mail address: eswar@iiti.ac.in (K.E. Prasad).

than the MG counterparts. NGs are fabricated using bottom-up approaches like magnetron sputtering, electroplating, and inert gas condensation [12–14]. The preliminary deformation experiments conducted on NGs show reasonably good plasticity compared to the MGs of identical composition [15–21]. The reason is attributed to the unique microstructure of NGs, which promotes nucleation of multiple shear bands, leading to strain partitioning and consequently avoiding plastic flow localization. Although there have been experimental studies characterizing the plastic flow characteristics of NGs, limited attention was given to investigating the effect of loading rate (or the strain rate) on the deformation behavior of NGs. One of the key characteristics of plastic deformation of materials is the *strain rate sensitivity, m*, as it provides useful information about the mechanisms of plastic flow.

The dependence of flow stress, σ, on the strain rate, $\dot{\varepsilon}$ is expressed by the power-law relation $\sigma = C\dot{\varepsilon}^m$ where C is a temperature-dependent material constant and m is strain rate sensitivity. The positive m values indicate homogeneous deformation, while the negative m indicate heterogeneous deformation. Besides qualitatively describing the nature of deformation, m is also used to quantify the activation volume needed for the plastic deformation. Conventionally, m is determined from the strain rate jump tests under uniaxial loading conditions, and recently it has been shown that m can also be obtained from the indentation experiments as $m = \frac{dlogH}{dlog\dot{\varepsilon}_i}$, where H and $\dot{\varepsilon}_i$ represents the indentation hardness and indentation strain rate, respectively. The $\dot{\varepsilon}_i$ is expressed as $\left(\frac{\dot{P}}{2P_{max}}\right)$, where $\dot{P}$ is the indentation loading rate and P_{max} is the maximum indentation load [22]. At room temperature, most of the engineering alloys display positive m values ranging between 0 and 0.1.

Several studies [23–37] have been conducted to investigate the m value of BMGs, and most of the studies, except a few [28–32], report negative m, while limited studies are available on MGs and NGs. Pan et al. [31] performed indentation strain rate jump experiments and observed that the H increases with loading rate, indicating positive m values. Using m values and the cooperating shearing model (CSM), they have determined the STZ volume, which is in the range of 2–7 nm^3 (containing a few 100′s atoms) for most BMGs. Recently, Boltynjuk et al. [32] observed a higher m in severely deformed Zr-based BMG than the as-cast BMG and attributed the positive m values to high STZ sites. Bhattacharyya et al. [33] argued that the positive m values are due to the experimental artifact and the possible reason for this is the overestimation of H without considering the pile-up around the impression, particularly at high indentation loads. Further, they argued that the negative m values are due to the lack of time (with increasing loading rate) for the material to relax the structure. Sort et al. [34] reasoned that the negative m values are due to the generation and accumulation of free volume at high loading rates. Recently, Sahu et al. [35] reported a negative m value for Ni_{60} Zr_{40} thin-film MG (containing fine crystals of 2–3 nm in size) and attributed it to a decrease in STZ size at high loading rates and relaxation mechanisms prevalent at low loading rates. In another study, Zhao et al. [36] reasoned that the time available for relaxation or diffusion is less at a higher loading rate, making the material softer, resulting in negative m. Recently, Gunti et al. [37] have also argued that higher loading rates caused significant activation of STZs and accredited the difference in the deformation behavior in mode to the strain rate fluctuations observed with increasing indentation depth. The negative m obtained from various literature studies is summarized and presented in Table 1. Most of the studies conducted to date are on the as-cast or deformed MGs and BMGs, but limited attention was given to understanding the strain rate sensitivity of NGs. Unlike the deformed MGs and BMGs, where the free volume is heterogeneously distributed, the NGs have a more uniformly distributed defect structure. Hence, it is interesting to investigate the strain rate sensitivity of NGs. This will not just only provide the key findings but will help us shed new light on understanding the deformation mechanisms of NG and provide novel guidelines for designing amorphous alloys with improved ductility.

Therefore, the current study is performed with the following objectives: (a) What is the effect of loading rate on NG and MG load vs. displacement response having identical composition? (b) How does the hardness vary with the loading rate? (c) What is the role of NG microstructure on m? and (d) How do m values of NGs fare with the MGs of an identical composition? To address the above questions, we have carried out nanoindentation experiments on a binary $Cu_{60}Zr_{40}$ MG and NG at different loading rates. In order to understand differences in shear band characteristics and the trend observed in m values between the NG and MG interface, microindentation experiments are performed as it is difficult to characterize the same using nanoindentation due to the limitations of maximum indentation load.

2. Material and experiments

$Cu_{60}Zr_{40}$ NG samples are produced in an inert-gas condensation (IGC) system, using binary $Cu_{60}Zr_{40}$ alloy as the sputtering target, while the binary $Cu_{60}Zr_{40}$ MG are synthesized using the melt-spinning technique. Both the NG and MG used in the current experiments are in as-processed condition without any subsequent annealing after their fabrication. The NG is disc-shaped with a thickness of ~0.3 mm and a diameter of 8 mm, and MG has a thickness of 30–40 µm, a width of ~1 mm, and a length of 10–20 mm. The amorphous nature of NG and MG is confirmed using X-ray diffraction (XRD). XRD was conducted using Cu-K_α radiation within the range of 2–70°. The surface of the samples is subsequently polished to a surface finish of 0.25 µm using the standard metallographic sample preparation method and then taken for indentation experiments. Nanoindentation experiments are performed at room temperature using a Hysitron Triboindenter with a Berkovich three side pyramidal-shaped diamond indenter. The experiments are conducted in a load-controlled mode at a maximum applied load of 4mN. The indentations are performed at different loading rates in the range of 0.26 mN/s to 8 mN/s, which corresponds to 3 decades of indentation strain rates. A minimum (4 ×4) array of 16 indents is taken at each load to obtain precise and reliable statistical data. The distance between the successive indents is kept about ten times the maximum indentation depth to circumvent the strain field interaction. The hardness, *H,* is determined using the Oliver and Pharr (O&P) method [38] as

$$H = \frac{P_{max}}{A_c} \tag{1}$$

Where P_{max} is the maximum indentation load, and A_c is the contact area, which is a function of contact depth, h_c. As per the O&P method, the h_c is given by Eq. (2);

$$h_c = h_{max} - \mu\frac{P_{max}}{S} \tag{2}$$

Here, h_{max} is the maximum penetration depth, μ is the geometry constant (~ 0.75, for Berkovich indenter), and S is the stiffness which is obtained from the slope of the unloading part of P vs. h curve as $S = dP/dh$. Finally, the modulus, E, is obtained using the Eq. (3):

$$E_s = (1 - \nu_s^2)\left[\left(\frac{2\sqrt{A_c}}{S\sqrt{\pi}}\right) - \left(\frac{1 - \nu_i^2}{E_i}\right)\right]^{-1} \tag{3}$$

where E and ν represent the elastic modulus, and Poisson's ratio and the subscripts i and s refer to the indenter and specimen, respectively. Before starting the experiment, the area function of the

Table 1
Summary of the m values reported for glasses in various literature.

Material	Structural state	Nature of test (Strain rate range, s^{-1})	Strain Rate Sensitivity, m	Ref.
$Zr_{52.5}Ti_5Cu_{17.9}Ni_{14.6}Al_{10}$ (Vitreloy105)	As-cast	Compression 3.3×10^{-3} - 3.7×10^{-4}	- 0.001 ± 0.0005	[23]
Vitreloy 105	As-cast	Compression test 2.34×10^{-3} - 1.87×10^{-1}	- 0.0026	[24]
$Pd_{40}Ni_{40}P_{20}$	As-cast	Compression 3.3×10^{-5} – 2×10^{3}	Negative	[25]
Vitreloy 105	As-cast	Compression 3.33×10^{-3} – 2×10^{-1}	-0.002	[26]
$Zr_{65}Cu_{20}Fe_5Al_{10}$	As-cast	Compression tests 5×10^{-3} – 5×10^{-2}	- 0.0026	[27]
$Zr_{41.2}Ti_{13.8}Cu_{12.5}Ni_{10}Be_{22.5}$	As-cast	Indentation tests @ P_{max} of 9 mN	-0.0166 ± 0.001	[33]
Vitreloy 1	Structurally relaxed	2.22×10^{-2} – 4.4×10^{-1}	-0.0201 ± 0.001	
	Shot peened		-0.0128 ± 0.001	
Vitreloy 1	As-cast	Indentation tests @ P_{max} of 250 mN	-0.0137 ± 0.001	[33]
	Structurally relaxed	3.33×10^{-3} – 2×10^{-1}	-0.0106 ± 0.001	
	Shot peened		-0.008 ± 0.001	
$Ti_{40}Zr_{25}Ni_8Cu_9Be_{18}$ BMG	As-cast	Indentation 2.5×10^{-3} – 1.25×10^{-1}	-0.063	[34]
$Ni_{60}Zr_{40}$ amorphous NG thin film	As-deposited	Indentation tests 0.01, 0.1 and 1 s^{-1}	-0.032 to – 0.057 (300 K) -0.021 to-0.039 (600 K)	[35]
$Pd_{40}Cu_{30}Ni_{10}P_{20}$	As-cast	Indentation tests @ P_{max} of 50, 100, 200 mN	Negative	[36]
$Zr_{48}Cu_{32}Ni_4Al_8Ag_8$		5×10^{-3} – 2.5×10^{-1}		
$Zr_{48}Cu_{34}Pd_2Al_8Ag_8$				
Vitreloy 1	As-cast	Indentation tests @ P_{max} of 500 mN	Negative	[37]
Vitreloy 105		1×10^{-3} – 1		
$Zr_{58.5}Cu_{15.6}Ni_{12.8}Al_{10.3}Nb_{2.8}$ (Vitreloy 106 A)				
Zr55Cu30Ni5Al10 (ZR55)				

indenter tip is calibrated with the help of a standard quartz sample by performing a series of indentations at different indentation depths.

Bonded interface indentation (BII) experiments are performed to qualitatively compare the differences in deformation characteristics beneath the indenter for both the NG and MG samples as they may provide reasons for the differences in m. Two specimens are taken with one of their surfaces polished up to 0.25 µm surface finish to perform the BII experiment. The polished surfaces are then bonded together by applying a strong adhesive ("super glue") and allowed to soak for 5 h. The specimens are then cold mounted in such a way that the bonded interface is on the top surface of the mould, which is again polished up to a surface finish of 0.25 µm. Following this, Vickers indentation is performed on the interface at a P_{max} of 3 N. The indentations are made in such a way that the diagonal of the imprint lies along with the interface. Subsequently, the bonded interface is opened by dissolving the super glue in acetone for 1–2 h and examined using a scanning electron microscope (SEM) to characterize the differences in shear band morphology underneath the indentation between the two glasses. Although we have used nanoindentation experiments to compute the m values, the micro-indentation was used for BII experiments due to the limitations of P_{max} in nanoindentation. Nevertheless, the BII experiments are performed under similar loading conditions (with the same load, loading rate, and indenter geometry) on both NG and MG to compare the shear band characteristics effectively.

3. Results

The XRD patterns of the as-prepared MG and NG samples are presented in Fig. 1, which shows a broad characteristic diffraction hump with no signatures of crystalline phases, confirming the presence of an amorphous structure. Fig. 2a and b show the typical P vs. h curves of NG and MG corresponding to different loading rates, i.e., 0.26, 0.4, 0.8, and 8 mN/s. The indentation imprints of NG and MG show no significant pile-up at the imprint edges, indicating that the O&P analysis can be suitably employed to determine the H [15,16]. According to the O&P analysis, the relation between the P and h of

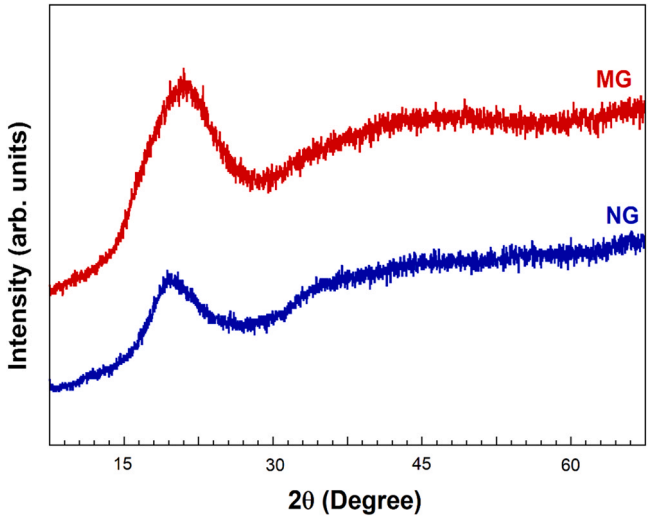

Fig. 1. X-ray diffraction spectra of the MG and NG samples.

the loading and unloading curves are described by the Eqs. (4 and 5) presented below:

$$P = \alpha h^{q} \tag{4}$$

$$P = \beta (h - h_f)^{r} \tag{5}$$

Where fitting constants α and β represent the resistance to indentation, and the elastic recovery of the material, q, and r represent the power-law exponents of loading and unloading curves, which depend on the indenter geometry, while h and h_f indicate the instantaneous and final penetration depth of the indenter, respectively. The loading and unloading curves of both NGs and MGs are well described by the Eqs. (4) and (5) (as presented in supplementary Fig. S1 and S2) with the regression coefficient values, $R^{2,}$ close to ~ 0.999. All the P vs. h curves (at different loading rates) yield similar power-law exponents approving a high level of reproducibility and repeatability of the nanoindentation results. The loading curves of

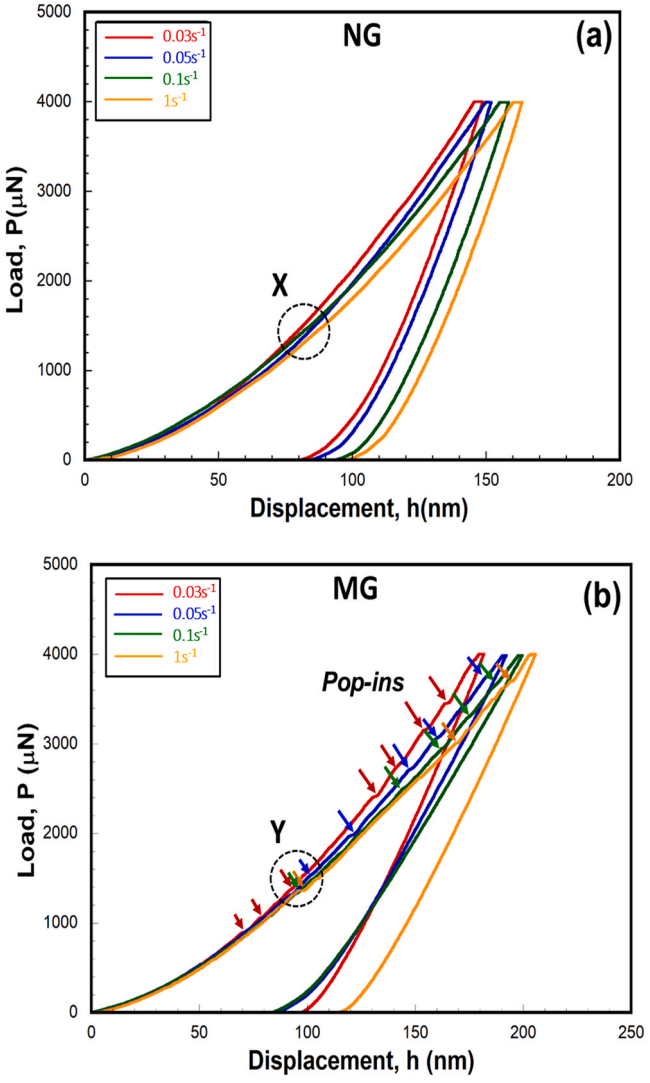

Fig. 2. Representative indentation load, *P* vs. penetration depth, *h* curves obtained under different loading rates for (a) NG and (b) MG at a P_{max} of 4 mN, respectively.

NG (as presented in Fig. 2a) exhibit smooth behaviour (characterized by the absence of displacement bursts or "*pop-ins*"), suggesting homogeneous plastic deformation. This observation is consistent with previous experimental studies reported for NGs [15–18,39–42]. Another interesting observation from Fig. 2a is the increase in penetration depth with loading rate suggesting softening of the material, and the reason for this behavior is discussed in detail in the subsequent sections. Contrastingly, the loading curves of MG samples (Fig. 2b) are characterized by a serrated flow, manifested by a large number of pop-ins (indicated by arrows), indicating the inhomogeneous nature of the deformation of MGs. A close examination of the loading segments reveals that the *pop-in* width decreases with an increase in loading rate for the MG, as shown in the magnified view in Fig. 3. Further, derivative technique is employed on the loading curves to characterize the pop-in behavior in detail as shown in supplementary figure Fig. S3 [43,44]. The plots dP/dh vs. h and dP/dh^2 vs. h^2 for MG are displayed in Fig. S3a and b, while for NG in c and d, respectively. The significant spikes observed in the horizontal line of Fig. S3 indicate the pop-ins occurring due to the nucleation of shear bands in MG. The intensity of spikes decreases with increasing strain rate, indicating the absence of severe flow localization. Such spikes are not observed in NG at all the strain rates suggesting a near homogeneous deformation. Further, the displacement bursts are quantified by measuring the *pop-in* width, $h_{\text{pop-in}}$, at different loading rates, and their average values are plotted as a function of the loading rate for NG and MG, as shown in Fig. 4. In order to determine the pop-in width, $h_{pop\text{-}in}$, the loading portion curves are magnified in the regions where there is a deviation from the power law. The horizontal distance between the start and end points from such regions yields, $h_{pop\text{-}in}$. The penetration depth corresponding to pop-ins are clearly identified from supplementary figure Fig. S3 of the revised manuscript. It is evident from Fig. 4 that for MGs, the $h_{\text{pop-in}}$ decreases with an increase in loading rate. A similar trend is reported for MGs and BMGs in the previous literature studies [34,36,45–47], which is attributed to the change in deformation mechanism from heterogeneous to homogeneous with an increase in loading rate. Interestingly, $h_{\text{pop-in}}$ remains nearly zero for NG, suggesting no substantial change in the deformation mechanism with increasing loading rate. The variation of H with the loading rate for both NG and MG obtained at P_{max} of 4 mN is plotted in Fig. 5a. It can be noticed from the figure that, at all the loading rates, NG exhibits a higher H than the MG, consistent with the previous experimental and simulation studies [15–17,48–51]. Besides this, the H decreases with an increased loading rate for both the NG and MG samples. The m values are obtained from the slope of H vs. equivalent strain rate plotted in the log-log scale (Fig. 5b) and are presented in Table 2. In both the glasses, the m value is found to be negative, but interestingly, its value for NG is more positive than the MG.

Further, the reasons for the observed differences in m values are examined using subsurface deformation zones of MG and NG as presented in Figs. 6 and 7, respectively. It is observed from Fig. 6 that the plastic strain in the subsurface deformation region of MG is mainly accommodated by large shear bands, known as primary shear bands (PSBs). The PSBs appear to be semi-circular in shape with no waviness at the shear band front having small and large curvatures. The shear bands having smaller at their front are much sharper suggesting unhindered propagation during the deformation, while the one with large curvature has a wavy front indicating their interaction with other bands during their propagation. The differences in curvatures of the shear bands possibly appeared due to diverse stress fields generated beneath the indenter during indentation [51,52]. Contrastingly, in the case of NGs, a large number of very fine shear bands, referred to as secondary shear bands (SSBs), are formed in between PSBs (Fig. 7). Unlike MGs, the shear bands front in NGs is wavy, which may be due to the multiple shear band interactions. The bands are diffused and thus making it difficult to differentiate the primary and secondary shear bands (SSBs). Similar observations have been reported in the case of binary Pd-Si MG and NG [16]. The primary and secondary shear bands are discernible in Pd-Si NGs, unlike the Cu-Zr NGs. In summary, the following observations can be made from the experimental results (a) The Cu-Zr NG shows a higher H as compared to the MG, having the identical composition (b) The *pop-ins* in the loading portion of P vs. h curves are dependent on the loading rate in MG while it has a no effect in NG (c) The penetration depth is found to increase with the increase in loading rate for both MG and NG indicating that both the glasses become softer with increasing loading rates. (d) The m computed from the nanoindentation data clearly shows a negative value for both MG and NG, albeit slightly more positive in NG than the MG. (e) The subsurface deformation zone in NG comprises several fine shear bands compared to the large shear bands in MG.

4. Discussion

In the following discussion and subsequent analysis, the effect of loading rate on the P vs. h response, H, and strain rate sensitivity is analyzed in light of STZ activity and the differences in shear band characteristics in the subsurface deformation zone between the two glasses.

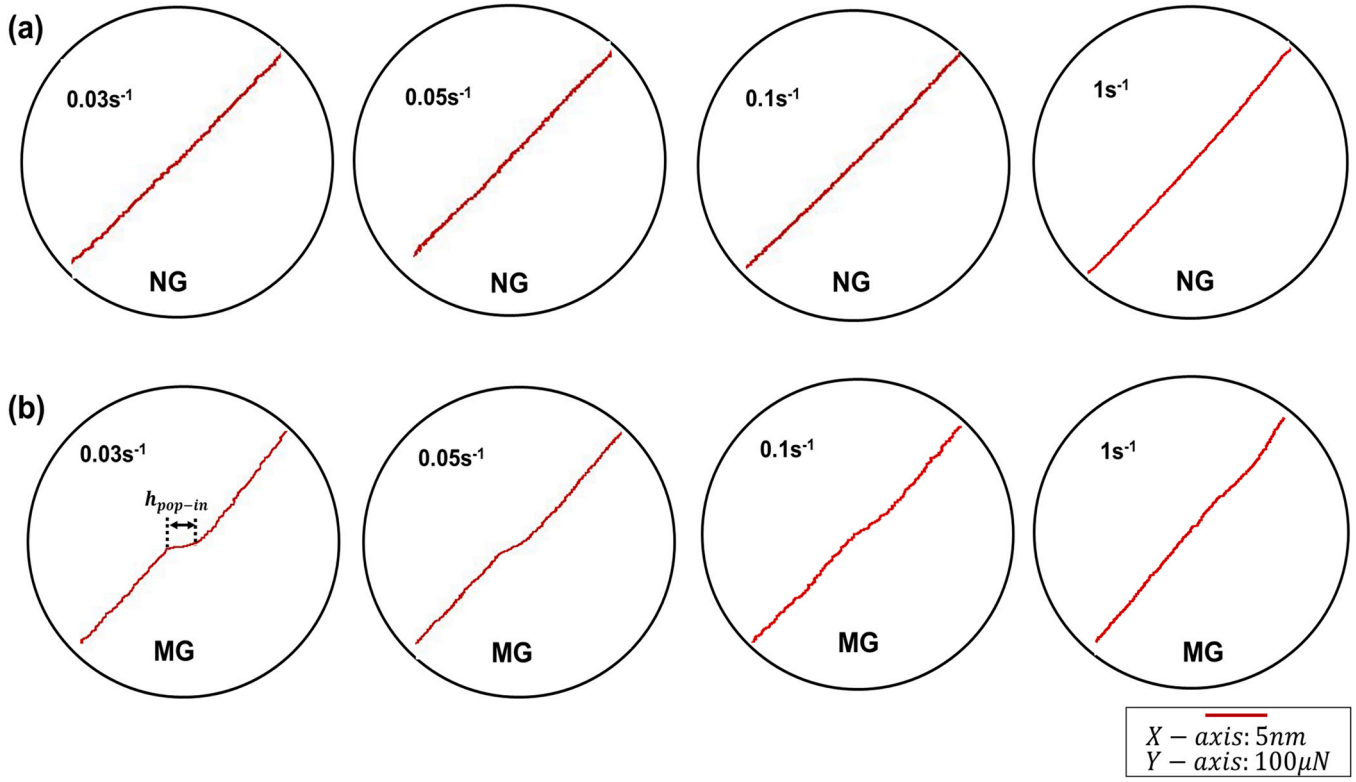

Fig. 3. Enlarged view of the loading portion of the *P* vs. *h* curves from regions X and Y at different loading rates for (a) NG and (b) MG respectively, describing the *pop-in* behaviour.

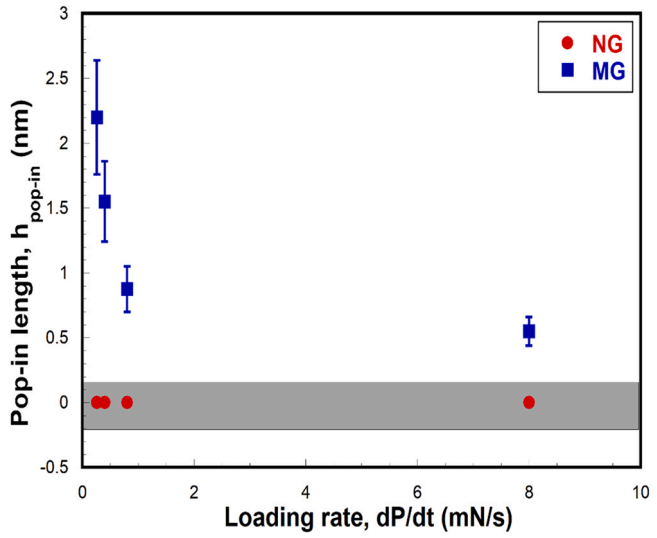

Fig. 4. Plot representing the variation of *pop-in* length, $h_{pop\text{-}in}$, with loading rate for NG and MG.

4.1. Analysis of P vs. h curves: effect of loading rate

The loading part of the *P* vs. *h* curve provides insights into the deformation events taking place underneath the indenter, and the smoother curve (i.e., the absence of *pop-ins*) indicates near homogeneous plastic flow. It has been observed in BMGs that temperature, strain rate, and structural state of the glass govern the *pop-in* behavior. Ramamurty and co-workers [53–57] carried out experiments on as-cast (AC), structurally relaxed (SR), and shot-peened (SP) BMGs and observed that SP BMG exhibited the lowest number of *pop-ins* in the loading curves, which was attributed to the presence of high free volume and nucleation of a large number of STZs. Schuh et al. [45–47] have developed a deformation mechanism map based on the indentation experiments with indentation strain rate and temperature as the abscissa and ordinate. According to this map, BMGs exhibit near homogeneous flow at high temperatures and high strain rates because of the dynamic relaxation processes prevalent under these experimental conditions. The post deformation images of the indentation imprints did not show any shear bands at the periphery of the impression confirming that the flow is homogenous. Jang et al. [58] have repeated indentation experiments under similar conditions (with T and $\dot{\varepsilon}$) with a cube-corner indenter and reported shear bands at the periphery of the imprint. They argued that the stress state underneath the indenter, besides the temperature and strain rate, also has a marked influence on the nature of deformation. One of the possible reasons for this could be the *cutting* type of plastic flow mechanism observed under the cube corner indenter in contrast to the *compression* type of mechanism in a Berkovich indentation. The absence of *pop-ins* in NGs at all the indentation loading rates is attributed to the high free volume containing regions and abundance of STZ nucleation sites [9]. In contrast, the decrease in the number of *pop-ins* in MGs with increasing loading rate is attributed to the difference in the dynamic relaxation processes around the indentation. Under low indentation loading rates, there is sufficient time for the material around the indenter to relax the structure in MG, which necessitates the nucleation of new shear bands or propagation of existing bands leading to *pop-ins* in the loading curve. Lack of time for the structural relaxation at high loading rates causes a local increase in free volume around the indenter, eventually leading to an absence of *pop-ins* in the loading curve.

4.2. Variation of hardness between the NG and MG

It is observed that the annealed (or structural relaxed) BMGs exhibit a higher *H* than the as-cast and shot-peened BMGs due to the presence of low free volume [54–56]. Following this, it is expected

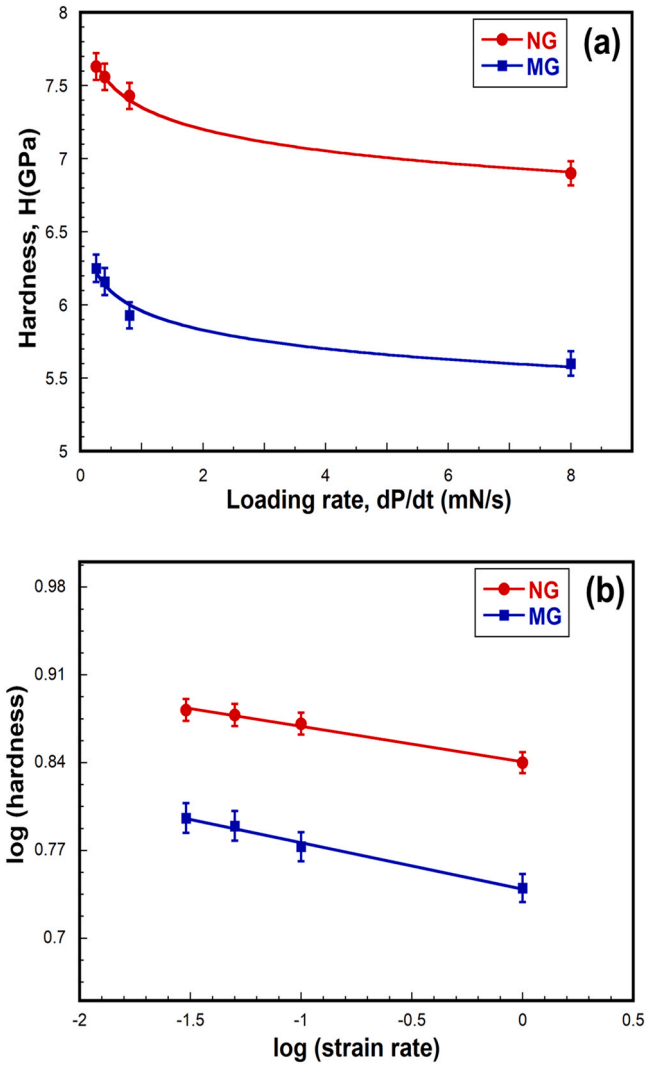

Fig. 5. Plot representing (a) the variation of hardness, H, with loading rate, dP/dt and (b) strain rate, $\dot{\varepsilon}$, plotted on log scale for NG and MG.

Table 2
Values of m obtained in present study for NG and MG.

Glass	Strain rate sensitivity, m @ P_{max} of 4mN
$Cu_{60}Zr_{40}$-NG	– 0.028 ± 0.002
$Cu_{60}Zr_{40}$-MG	– 0.037 ± 0.003

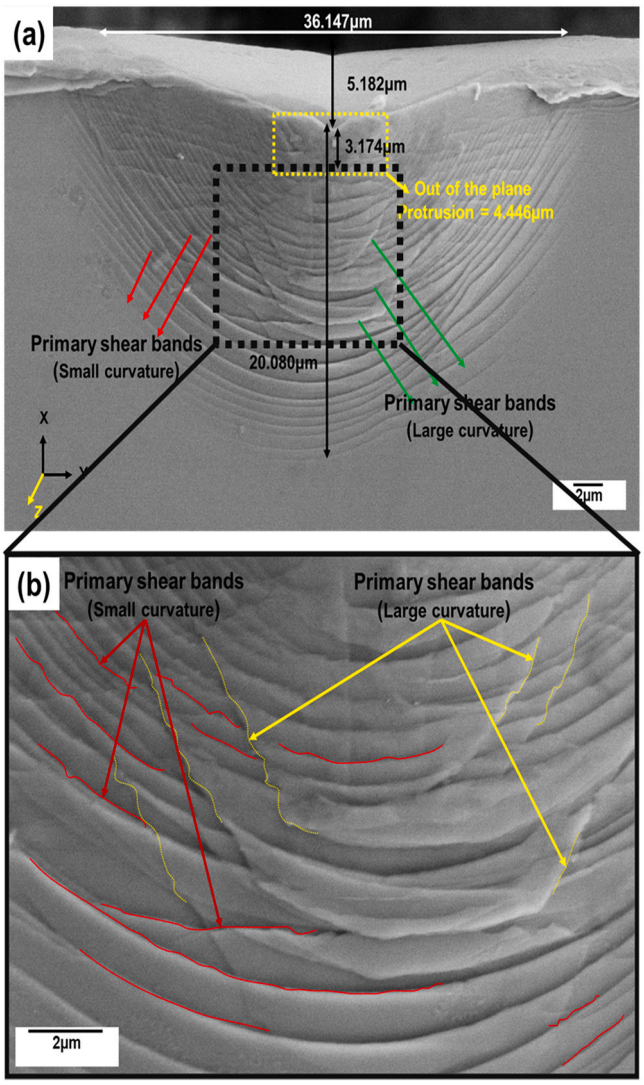

Fig. 6. Subsurface deformation zone of a $Cu_{60}Zr_{40}$ MG at a P_{max} of 3 N obtained at a loading rate of 0.3 N/s (an equivalent strain rate of 0.1 s^{-1}) indicating (a) complete deformation zone and (b) a high magnification image of the highlighted region of (a).

that Cu-Zr NGs should exhibit a lower H as compared to MGs, contrary to the current experimental results (Table 3) observed in the current study. The possible reasons for this could be attributed to the (*i*) compositional segregation prevalent in the nanoparticles during their fabrication in NGs, (*ii*) increased pressure sensitivity of NGs and (iii) presence of icosahedra clusters in the interfacial regions. In $Cu_{60}Zr_{40}$ NG (rich in Cu content), a higher T_g and T_x are observed due to the segregation of Cu to the interfacial regions of GGs with the core rich in Zr [9–11,15,50]. These Cu particles are prone to form icosahedra clusters leading to an increase in medium-range ordering (MRO) in the interfacial regions. These clusters offer greater resistance to plastic deformation, thereby increasing the H of NGs. Recently, it has been observed that the number of clusters and their size can be varied by thermal annealing, which influences the β relaxation kinetics and mechanical properties [16,59,60]. Further, the high free volume present in the GIs also causes an increase in pressure sensitivity index during the plastic deformation, thereby leading to an increase in the hardness of NGs [48]. With the help of a modified expanding cavity model applicable, Narasimhan [61] has observed higher H in materials having higher pressure sensitivity index due to the large elasticity continuum surrounding the indentation zone.

4.3. Strain rate sensitivity of NGs and MGs and its structural dependence

The negative m for both the NGs and MGs shows that the deformation is heterogeneous in both the glasses, consistent with the observations reported for BMGs [23–27]. Between the two, NGs exhibit more positive m values as compared to the MGs, and these differences in m are attributed to the variation in the internal microstructures. In both NG and MG, the fundamental carriers of plasticity are STZs, but they differ in their number density, and the volume (number of atoms present in the STZ). Pan et al. [31] have measured the STZ volume and number of atoms present in the STZ for a number of BMGs using the co-operative shearing model (CSM). For a $Cu_{60}Ti_{25}Hf_{15}$ (which is stoichiometrically closer to the glasses used in the current study), the STZ volume is 4.23 nm^3 with 359 atoms. After rigorous evaluation of the indentation impressions,

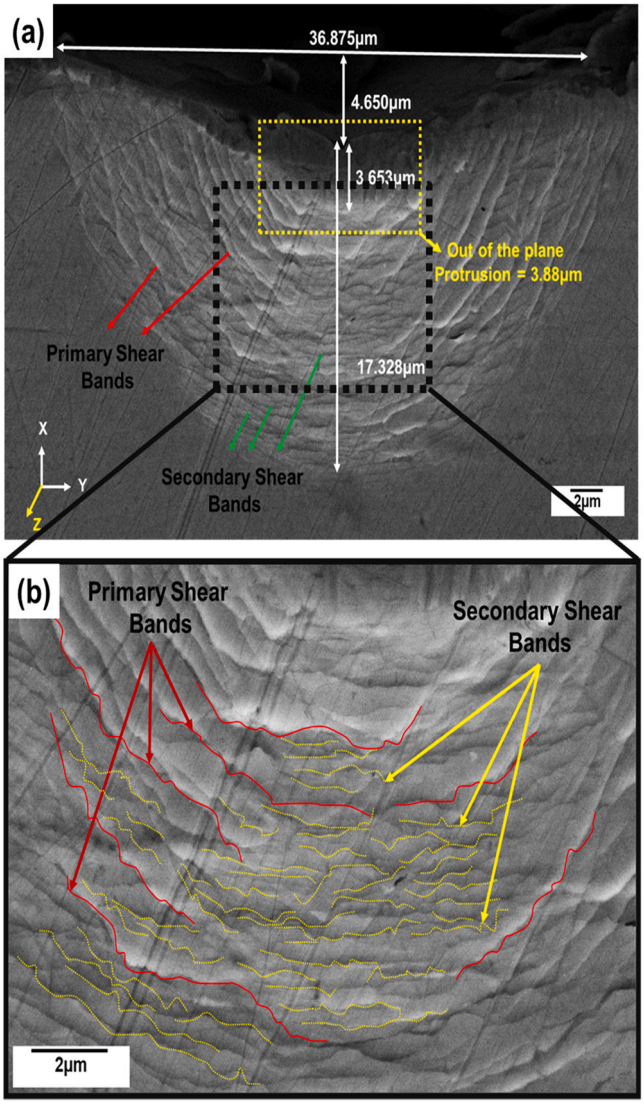

Fig. 7. Subsurface deformation zone of a $Cu_{60}Zr_{40}$ NG at P_{max} of 3 N at a loading rate of 0.3 N/s indicating (a) complete deformation zone and (b) a high magnification image of the highlighted region.

Table 3
- Summary of nanomechanical properties and elastic recovery obtained from the analysis of load, P vs. displacement, h curves.

Strain rate, s^{-1}	Nanohardness, H (GPa)		Elastic modulus, E (GPa)	
	NG	MG	NG	MG
0.03	7.63 ± 0.10	6.25 ± 0.12	109 ± 1.8	51.8 ± 1.5
0.05	7.56 ± 0.15	6.16 ± 0.10	112 ± 1.0	52.6 ± 1.2
0.1	7.43 ± 0.12	5.93 ± 0.12	112 ± 2.5	51.3 ± 2.2
1	6.90 ± 0.15	5.60 ± 0.11	112 ± 1.5	54.5 ± 1.0

Bhattacharyya et al. [33] noticed that the positive *m* in BMGs is indeed an experimental artifact due to the pile-up of the material around the impression. Choi et al. [62] have later computed the STZ volume for an as-cast and annealed Zr-based BMG (Vit 105), considering the first *pop-in* load which is found to be 0.347 and 0.464 nm^3, respectively, suggesting that structural relaxation increases the size of STZ. Using the same procedure, Tao et al. [63] analyzed the STZ size in a $Zr_{50}Cu_{40}Al_{10}$ BMG in three different structural states (as-cast, annealed, and plastically deformed) and observed it to be 0.43, 0.55, and 0.34 nm^3, respectively. These studies clearly show that STZ size depends on the structural state, which

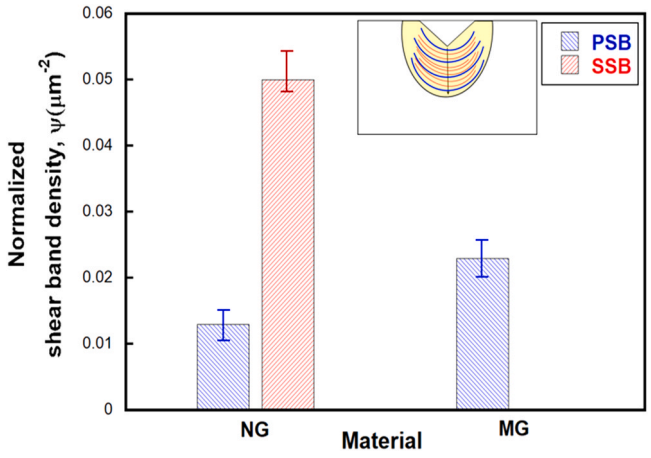

Fig. 8. Variation of normalized primary and secondary shear band density, Ψ, in the subsurface deformation zone for NG and MG.

decreases with decreasing free volume content. Nandam et al. [15] have also computed the STZ volume in $Cu_{50}Zr_{50}$ NG and MG as 7.41 and 1.93 nm^3, respectively, based on the positive *m* value, which are much higher than the predictions of BMG. One of the possible reasons for this could be due to the high nanoindentation load (25 mN) and the use of *H* not corrected for *pile-up*. Since the NGs do not contain *pop-ins* in the loading curve, it is impossible to compute the STZ volume based on the first pop-in load, which also implies that the STZ volume in NGs must be much smaller than the ones predicted for severely deformed BMG. The subsurface deformation zone presented in Figs. 6 and 7 (performed under identical loading conditions) highlights the relative difference in shear band characteristics between the MGs and NGs, although it is not a true representation of constrained indentation based on which the *m* values are computed. The shear band density, Ψ, is calculated as the number of primary and secondary shear bands (PSBs and SSBs, respectively) per unit deformation area and plotted for NG and MG in Fig. 8. It is observed that the Ψ of PSBs in NG, unlike MGs, is very small compared to the SSBs. The increased Ψ of SSBs is indicative of a large number of STZ nucleation sites, thereby reducing the propensity of heterogeneous deformation. In a nutshell, the less negative *m* values of NG indicate an increased tendency for homogeneous nature deformation, which could be attributed to the high free volume (and concomitant availability of a large number of STZs). A detailed investigation of the STZ size in NGs is warranted to understand the origins of reduced m values further. Advanced characterization techniques are needed to resolve further the STZ volume in NGs, which may provide further insights into the deformation behavior of NGs and ways to enhance the plasticity of glasses.

5. Conclusions

$Cu_{60}Zr_{40}$ nano- and metallic glasses are synthesized using IGC and melt spun technique, respectively, and their strain rate sensitivity over three decades of strain rates is investigated using nanoindentation. Further, the deformation characteristics in the subsurface deformation zone are analyzed using bonded interface indentation. The following conclusions can be drawn from the current results:

- The serrated flow in the loading curves of MGs decreases with an increase in loading rate while it does not have any effect on the NGs. NGs do not exhibit serrated flow at any indentation loading rate.
- The hardness of both the NG and MG decreases with increasing loading rate implying negative strain rate sensitivity, *m*. The *m*

values of NG are higher than the MG, indicating a tendency towards the near homogeneous plastic flow. Despite the high hardness in NGs, the high free volume is due to icosahedra clusters present at the interfaces.

- The primary shear bands (PSBs) are the main carriers of plastic flow in MG, while in NG, owing to the high free volume, it is by secondary shear bands (SSBs). The relatively positive *m* in NG compared to the MG is attributed to a large number of fine shear bands and near homogeneous plastic deformation.

CRediT authorship contribution statement

Sharma: Conceptualization, Investigation, Formal analysis, Writing – original draft. **S.S. Hirmukhe:** Investigation. **S. H. Nandam:** Methodology, Investigation. **H. Hohn:** Supervision, Project administration, Resources. **I. Singh:** Supervision. **R.L. Narayan**: Formal analysis. **K. Eswar Prasad**: Methodology, Supervision, Project administration, Funding acquisition, Resources, Writing – review & editing.

Data Availability

Data will be made available on request.

Declaration of Competing Interest

The authors declare that they have no known competing financial interests or personal relationships that could have appeared to influence the work reported in this paper.

Acknowledgments

The authors would like to thank Prof. Rajesh Korla and Mr. Sairam for the help rendered in conducting the nanoindentation experiments. The department of MEMS, IIT Indore, is also acknowledged for providing the characterization facilities used in the current study.

Appendix A. Supporting information

Supplementary data associated with this article can be found in the online version at doi:10.1016/j.jallcom.2022.165991.

References

[1] C.A. Schuh, T.C. Hufnagel, U. Ramamurty, Mechanical behavior of amorphous alloys, Acta Mater. 55 (2007) 4067–4109, https://doi.org/10.1016/j.actamat.2007.01.052
[2] M.L. Falk, J.S. Langer, Dynamics of viscoplastic deformation in amorphous solids, Phys. Rev. E 57 (1998) 7192, https://doi.org/10.1103/physreve.57.7192
[3] S.X. Song, Y.H. Lai, J.C. Huang, T.G. Nieh, Homogeneous deformation of Au-based metallic glass micropillars in compression at elevated temperatures, Appl. Phys. Lett. 94 (2009) 061911, https://doi.org/10.1063/1.3081111
[4] K.E. Prasad, U. Ramamurty, Effect of temperature on the plastic zone size and the shear band density in a bulk metallic glass. Mater, Sci. Eng.:A 535 (2012) 48–52.
[5] C.C. Hays, C.P. Kim, W.L. Johnson, Microstructure controlled shear band pattern formation and enhanced plasticity of bulk metallic glasses containing in situ formed ductile phase dendrite dispersions, Phys. Rev. Lett. 84 (2000) 2901–2904.
[6] H. Gleiter, Nanoglasses: a new kind of noncrystalline materials, Beilstein J. Nanotechnol. 4 (2013) 517–533, https://doi.org/10.3762/bjnano.4.61
[7] Y. Ivanisenko, C. Kubel, S.H. Nandam, C. Wang, X. Mu, O. Adjaoud, K. Albe, H. Hahn, Structure and properties of nanoglasses, Adv. Eng. Mater. 20 (2018) 1800404, https://doi.org/10.1002/adem.201800404
[8] L. Deng, K. Kosiba, R. Limbach, L. Wondraczek, U.K. uhn, S. Pauly, Plastic deformation of a Zr-based bulk metallic glass fabricated by selective laser melting, J. Mat. Sci. Technol. 60 (2021) 139–146, https://doi.org/10.1016/j.jmst.2020.06.007
[9] Y. Ritter, D. Sopu, H. Gleiter, K. Albe, Structure, stability and mechanical properties of internal interfaces in Cu64Zr36 nanoglasses studied by MD simulations, Acta Mater. 59 (2011) 6588–6593, https://doi.org/10.1016/j.actamat.2011.07.013
[10] O. Adjaoud, K. Albe, Influence of microstructural features on the plastic deformation behavior of metallic nanoglasses, Acta Mater. 168 (2019) 393–400, https://doi.org/10.1016/j.actamat.2019.02.033
[11] O. Adjaoud, K. Albe, Interfaces and interphases in nanoglasses: surface segregation effects and their implications on structural properties, Acta Mater. 113 (2016) 284, https://doi.org/10.1016/j.actamat.2016.05.002
[12] R. Witte, T. Feng, J.X. Fang, A. Fischer, M. Ghafari, R. Kruk, R.A. Brand, D. Wang, H. Hahn, H. Gleiter, Evidence for enhanced ferromagnetism in an iron-based nanoglass, Appl. Phys. Lett. 103 (2013) 073106, https://doi.org/10.1063/1.4818493
[13] N. Chen, R. Frank, N. Asao, D.V. Louzguine-Luzgin, P. Sharma, J.Q. Wang, G.Q. Xie, Y. Ishikawa, N. Hatakeyama, Y.C. Lin, M. Esashi, Y. Yamamoto, A. Inoue, Formation and properties of Au-based nanograined metallic glasses, Acta Mater. 59 (2011) 6433–6440, https://doi.org/10.1016/j.actamat.2011.07.007
[14] Z. Sniadecki, D. Wang, Y. Ivanisenko, V.S.K. Chakravadhanula, C. Kubel, H. Hahn, H. Gleiter, Nanoscale morphology of Ni50Ti45Cu5 nanoglass, Mater. Charact. 113 (2016) 26–33, https://doi.org/10.1016/j.matchar.2015.12.025
[15] S.H. Nandam, Y. Ivanisenko, R. Schwaiger, Z. Sniadecki, X. Mu, D. Wang, R. Chellali, T. Boll, A. Kilmametov, T. Bergfeldt, H. Gleiter, H. Hahn, Cu-Zr nanoglasses: atomic structure, thermal stability and indentation properties, Acta Mater. 136 (2017) 181–189, https://doi.org/10.1016/j.actamat.2017.07.001
[16] A. Sharma, S.H. Nandam, H. Hahn, K.E. Prasad, Effect of structural relaxation on the indentation size effect and deformation behavior of Cu-Zr-based nanoglasses, Frontiers 8 (2021) 676764, https://doi.org/10.3389/fmats.2021.676764
[17] A. Sharma, S.H. Nandam, H. Hahn, K.E. Prasad, On the differences in shear band characteristics between a binary Pd-Si metallic and nanoglass, Scr. Mater. 191 (2021) 17–22, https://doi.org/10.1016/j.scriptamat.2020.09.009
[18] S.H. Nandam, O. Adjaoud, R. Schwaiger, Y. Ivanisenko, M.R. Chellali, D. Wang, K. Albe, H. Hahn, Influence of topological structure and chemical segregation on the thermal and mechanical properties of Pd-Si nanoglasses, Acta Mater. 193 (2020) 252–260, https://doi.org/10.1016/j.actamat.2020.03.021
[19] X.L. Wang, F. Jiang, H. Hahn, J. Li, H. Gleiter, J. Sun, J.X. Fang, Plasticity of a scandium-based nanoglass, Scr. Mater. 98 (2015) 40–43, https://doi.org/10.1016/j.scriptamat.2014.11.010
[20] X.L. Wang, F. Jiang, H. Hahn, J. Li, H. Gleiter, J. Sun, J. Fang, Sample size effects on strength and deformation mechanism of Sc75Fe25 nanoglass and metallic glass, Scr. Mater. 116 (2016) 95–99, https://doi.org/10.1016/j.scriptamat.2016.01.036
[21] S.H. Nandam, R. Schwaiger, A. Kobler, C. Kubel, C. Wang, Y. Ivanisenko, H. Hahn, Controlling shear band instability by nanoscale heterogeneties in metallic nanoglasses, J. Mater. Res 36 (2021) 2903–2914, https://doi.org/10.1557/s43578-021-00285-4
[22] G.E. Dieter, D. Bacon, Mechanical Metallurgy, Metric (Ed.), McGraw-Hill, New York, 1986.
[23] Florian H.Dalla Torre, Alban Dubach, Marco E. Siegrist, J.örg F. Löffler, Negative strain rate sensitivity in bulk metallic glass and its similarities with the dynamic strain aging effect during deformation, Appl. Phys. Lett. 89 (2006) 091918, https://doi.org/10.1063/1.2234309
[24] W.H. Jiang, F.X. Liu, F. Jiang, K.Q. Qiu, H. Choo, P.K. Liaw, Strain-rate dependence of hardening and softening in compression of a bulk-metallic glass, J. Mater. Res. 22 (2007) 2655–2658.
[25] T. Mukai, T.G. Nieh, Y. Kawamura, A. Inoue, K. Higashi, Effect of strain rate on compressive behavior of a $Pd_{40}Ni_{40}P_{20}$ bulk metallic glass, Intermetallics 10 (2002) 1071, https://doi.org/10.1016/s0966-9795(02)00137-1
[26] A. Dubach, F.H. Dalla Torre, J.F. Löffler, Constitutive model for inhomogeneous flow in bulk metallic glasses, Acta Mater. 57 (2009) 881–892, https://doi.org/10.1016/j.actamat.2008.10.027
[27] S. Gonzalez, G.Q. Xie, D.V. Louzguine-Luzgin, J.H. Perepezko, A. Inoue, Deformation and strain rate sensitivity of a Zr-Cu-Fe-Al metallic glass, Mater. Sci. Eng. A 528 (2011) 3506–3512, https://doi.org/10.1016/j.msea.2011.01.049
[28] M. Li, Effect of annealing on strain rate sensitivity of metallic glass under nanoindentation, Metals 10 (2020) 1063, https://doi.org/10.3390/met10081063
[29] X. Wang, Z.Q. Ren, W. Xiong, S.N. Liu, Y. Liu, S. Lan, J.T. Wang, Negative strain rate sensitivity induced by structure heterogeneity in Zr64.13Cu15.75Ni10.12Al10 bulk metallic glass, Metals 11 (2021) 339, https://doi.org/10.3390/met11020339
[30] C. Ma, S. Li, P. Huang, F. Wang, Size dependent hidden serration behaviors of shear banding in metallic glass thin films, J. Non Cryst. Solids 534 (2020) 119953, https://doi.org/10.1016/j.jnoncrysol.2020.119953
[31] D. Pan, A. Inoue, T. Sakurai, M.W. Chen, Experimental characterization of shear transformation zones for plastic flow of bulk metallic glasses, PNAS 105 (2008) 14769–14772, https://doi.org/10.1073/pnas.0806051105
[32] E.V. Boltynjuk, D.V. Gunderov, E.V. Ubyivovk, M.A. Monclús, L.W. Yang, J.M. Molina- Aldareguia, A.I. Tyurin, A. Kilmametov, A.A. Churakova, A. Yu Churyumov, R.Z. Valiev, Enhanced strain rate sensitivity of Zr-based bulk metallic glasses subjected to high pressure torsion, J. Alloy. Compd. 747 (2018) 595–602, https://doi.org/10.1016/j.jallcom.2018.03.018
[33] A. Bhattacharyya, G. Singh, K.E. Prasad, R. Narasimhan, U. Ramamurty, On the strain rate sensitivity of plastic flow in metallic glasses, Mater. Sci. Eng.:A 625 (2015) 245–251.
[34] J. Sort, J. Fornell, W. Li, S. Surinach, M.D. Baro, Influence of the loading rate on the indentation response of Ti-based metallic glass, J. Mater. Res. 24 (2008) 918–925.
[35] B.P. Sahu, A. Dutta, R. Mitra, Mechanism of negative strain rate sensitivity in metallic glass film, J. Alloy. Compd. 784 (2019) 488–499.
[36] M.S.Z. Zhao, Z.L. Long, L. Peng, Nanoindentation studies of strain rate sensitivities in bulk metallic glasses, J. Non-Cryst. Solids 565 (2021) 150852, https://doi.org/10.1016/j.jnoncrysol.2021.120852
[37] A. Gunti, J. Das, Effect of testing conditions on the nanomechanical behavior of surface and inner core of as-cast Zr-base bulk metallic glassy plates, Mater. Sci. Eng. A 845 (2022) 143206, https://doi.org/10.1016/j.msea.2022.143206

[38] W.C. Oliver, G.M. Pharr, An improved technique for determining hardness and elastic modulus using load and displacement sensing indentation experiments, J. Mater. Res. 7 (1992) 1564–1583, https://doi.org/10.1557/JMR.1992.1564
[39] M.C. Li, M.Q. Jiang, F. Jiang, L. He, J. Sun, Testing effects on hardness of a Zr-based metallic glass under nanoindentation, Scr. Mater. 138 (2017) 120–123.
[40] S.S. Hirmukhe, A. Sharma, Sree Harsha Nandam, Horst Hahn, K.E. Prasad, I. Singh, Investigation of softening induced indentation size effect in Nanoglass and Metallic glass, J. Non-Cryst. Solids 577 (2022) (2022) 121316, https://doi.org/10.1016/j.jnoncrysol.2021.121316
[41] J.J. Pang, M.J. Tan, K.M. Liew, C. Shearwood, Nanoindentation study of size effect and loading rate effect on mechanical properties of a thin film metallic glass Cu49.3Zr50.7, Phys. B 407 (2012) 340–346, https://doi.org/10.1016/j.physb.2011.10.050
[42] A. Rauf, C.Y. Guo, Y.N. Fang, Z. Yu, B.A. Sun, T. Feng, Binary Cu-Zr thin film metallic glasses with tunable nanoscale structures and properties, J. Non-Cryst. Solids 498 (2018) 95–102, https://doi.org/10.1016/j.jnoncrysol.2018.06.015
[43] M. McGurk, T. Page, Using the P–δ^2 analysis to deconvolute the nanoindentation response of hard-coated systems, J. Mater. Res 14 (1999) 2283–2295, https://doi.org/10.1557/JMR.1999.0305
[44] J. Malzbender, G. de With, The use of the indentation loading curve to detect fracture of coatings, Surf. Coat. Technol. 137 (2001) 72–76, https://doi.org/10.1016/s0257-8972(00)01091-4
[45] C.A. Schuh, T.G. Nieh, A nanoindentation study of serrated flow in bulk metallic glasses, Acta Mater. 51 (2003) 87–99, https://doi.org/10.1016/S 13 59 -6454(02)00303-8
[46] C.A. Schuh, A.C. Lund, T.G. Nieh, New regime of homogeneous flow in the deformation map of metallic glasses: elevated temperature nanoindentation experiments and mechanistic modelling, Acta Mater. 52 (2004) 5879–5891, https://doi.org/10.1016/j.actamat.2004.09.005
[47] C.A. Schuh, T.G. Nieh. A survey of instrumented indentation studies on metallic glasses. J. Mater. Res. 19(1), 46–57, https://doi.org/10.1557/jmr.2004.19.1.46.
[48] S.S. Hirmukhe, K.E. Prasad, I. Singh, Investigation of pressure sensitive plastic flow in nanoglasses from finite element simulations, Scr. Mater. 180 (2020) 45–50, https://doi.org/10.1016/j.scriptamat.2020.01.022
[49] O. Franke, D. Leisen, H. Gleiter, H. Hahn, Thermal and plastic behavior of nanoglasses, J. Mater. Res. 29 (2014) 1210–1216, https://doi.org/10.1557/jmr.2014.101
[50] O. Adjaoud, K. Albe, Nanoindentation of nanoglasses tested by molecular dynamics simulations: influence of structural relaxation and chemical segregation on the mechanical response, Front. Mater. 8 (2021) 664220, https://doi.org/10.3389/fmats.2021.664220
[51] S. Xie, E.P. George, Hardness and shear band evolution in bulk metallic glasses after plastic deformation and annealing, Acta Mater. 56 (2008) 5202–5213, https://doi.org/10.1016/j.actamat.2008.07.009
[52] G. Subhash, H. Zhang. Dynamic indentation response of ZrHf-based bulk metallic glasses, J. Mater. Res. 22(02), 478–485, https://doi.org/10.1557/JMR.2007.0058.
[53] B.G. Yoo, K.W. Park, J.C. Lee, U. Ramamurty and J. Jang. Role of free volume in strain softening of as-cast and annealed bulk metallic glass. J. Mater. Res., 24(04) 1405–1416, https://doi.org/10.1557/JMR.2009.0167.
[54] R. Raghavan, R. Ayer, H.W. Jin, C.N. Marzinsky, U. Ramamurty, Effect of shot peening on the fatigue life of a Zr-based bulk metallic glass, Scr. Mater. 59 (2008) 167–170, https://doi.org/10.1016/j.scriptamat.2008.03.009
[55] R. Bhowmick, R. Raghavan, K. Chattopadhyay, U. Ramamurty, Plastic flow softening in a bulk metallic glass, Acta Mater. 54 (2006) 4221, https://doi.org/10.1016/j.actamat.2006.05.011
[56] A. Dubach, R. Raghavan, J.F. Löffler, J. Michler, U. Ramamurty, Micropillar compression studies on a bulk metallic glass in different structural states, Scr. Mater. 60 (2009) 567–570, https://doi.org/10.1016/j.scriptamat.2008.12.013
[57] U. Ramamurty, S. Jana, Y. Kawamura, K. Chattopadhyay, Hardness and plastic deformation in a bulk metallic glass, Acta Mater. 53 (2005) 705–717, https://doi.org/10.1016/j.actamat.2004.10.023
[58] J. Jang, B.G. Yoo, Y.J. Kim, Rate-dependent inhomogeneous-to-homogeneous transition of plastic flows during nanoindentation of bulk metallic glasses: fact or artifact? Appl. Phys. Lett. 90 (2007) 211906, https://doi.org/10.1063/1.2742286
[59] D. Sopu, K. Albe, Enhancing the plasticity of metallic glasses: shear band formation, nanocomposites and nanoglasses investigated by molecular dynamics simulations, Mech. Mater. 67 (2015) 94–103, https://doi.org/10.1016/j.mechmat.2013.06.004
[60] D. Sopu, Y. Ritter, H. Gleiter, K. Albe, Deformation behavior of bulk and nanostructured metallic glasses studied via molecular dynamics simulations, Phys. Rev. B 83 (2011) 100202, https://doi.org/10.1103/PhysRevB.83.100202
[61] R. Narasimhan, Analysis of indentation of pressure sensitive plastic solids using the expanding cavity model, Mech. Mater. 36 (2004) 633–645, https://doi.org/10.1016/s0167-6636(03)00075-9
[62] I. Choi, Y. Zhao, Y. Kim, B.G. Yoo, J.Y. Suh, U. Ramamurty, J. Jang, Indentation size effect and shear transformation zone size in a bulk metallic glass in two different structural states, Acta Mater. 60 (2012) 6862–6868, https://doi.org/10.1016/j.actamat.2012.08.061
[63] K. Tao, J.C. Qiao, Q.F. He, K.K. Song, Y. Yang, Revealing the structural heterogeneity of metallic glass: mechanical spectroscopy and nanoindentation experiments, Int. J. Mech. Sci. 201 (2021) 106469, https://doi.org/10.1016/j.ijmecsci.2021.106469